COMPUTER METHODS AND PROGRAMS IN BIOMEDICINE 113 (2014) 757–766

journal homepage: www.intl.elsevierhealth.com/journals/cmpb

A novel method for pulmonary embolism detection in CTA images

Haydar Özkan[a,*], *Onur Osman*[b], *Sinan Şahin*[c], *Ali Fuat Boz*[d]

[a] *Fatih Sultan Mehmet Vakıf University, Department of Biomedical Engineering, Istanbul, Turkey*
[b] *Arel University, Department of Electrical and Electronics Engineering, Istanbul, Turkey*
[c] *Dr. Siyami Ersek Thoracic and Cardiovascular Surgery Training and Research Hospital, Department of Radiology, Istanbul, Turkey*
[d] *Sakarya University Technology Faculty, Department of Electrical and Electronics Engineering, Sakarya, Turkey*

ARTICLE INFO

Article history:
Received 2 July 2013
Received in revised form
19 December 2013
Accepted 20 December 2013

Keywords:
Computed tomography angiography (CTA)
Lung segmentation
Lung vessel segmentation
Pulmonary embolism (PE)
Computer aided detection (CAD)

ABSTRACT

In this paper, we propose a new computer-aided detection (CAD) – based method to detect pulmonary embolism (PE) in computed tomography angiography images (CTAI). Since lung vessel segmentation is the main objective to provide high sensitivity in PE detection, this method performs accurate lung vessel segmentation. To concatenate clogged vessels due to PEs, the starting region of PEs and some reference points (RPs) are determined. These RPs are detected according to the fixed anatomical structures. After lung vessel tree is segmented, the region, intensity, and size of PEs are used to distinguish them. We used the data sets that have heart disease or abnormal tissues because of lung disease except PE in this work. According to the results, 428 of 450 PEs, labeled by the radiologists from 33 patients, have been detected. The sensitivity of the developed system is 95.1% at 14.4 false positive per data set (FP/ds). With this performance, the proposed CAD system is found quite useful to use as a second reader by the radiologists.

1. Introduction

PE is a difficult disease to diagnose clinically since many other conditions share the same symptoms [1]. It is a common disorder with a high morbidity and mortality for which an early and precise diagnosis is desirable [2]. The diagnostic imaging method of choice for the detection of PE in most institutions is contrast-enhanced pulmonary multi detector CT angiography (CTA) [3–6]. In the CTA images, the blood vessels appear to be very bright because the contrast material is dissolved in the blood. The embolus does not absorb this material, and thus it can be recognized in the CTA as a dark area in the pulmonary arteries. However, manual detection of the dark spots that correspond to PE in the CTA images is often described by radiologists as troublesome and time consuming [7].

CAD based on quantitative image analysis is one of the most important diagnosis methods [8,9]. In previous works, lung segmentation serves as the first implementation for some lung disease detection. In some of them, lung is segmented to detect lung nodules [10,11] and to classify lung cancer [12]. In this study, lung is segmented to segment lung vessels and to detect PEs. To perform segmentation in 3D images, conventional image processing methods are carried

* *Corresponding author at*: Fatih Sultan Mehmet Vakıf University, Faculty of Engineering & Architecture, Department of Biomedical Engineering, Haliç Campus, Sütlüce Mah. Karaağaç Cad. No: 12 Beyoğlu, Istanbul, Turkey. Tel.: +90 212 369 81 62; fax: +90 212 369 81 64; mobile: +90 543 882 37 70.
E-mail addresses: haydarozkan79@gmail.com, hozkan@fsm.edu.tr (H. Özkan).
0169-2607/$ – see front matter © 2013 Elsevier Ireland Ltd. All rights reserved.
http://dx.doi.org/10.1016/j.cmpb.2013.12.014

out. Carotid artery segmentation was carried out by Hassan at al. using modified spatial fuzzy c-means [13] and by Rocha at al. using random sample consensus (RANSAC) algorithm [14]. Also abdominal aortic aneurysm segmentation was achieved by Zohios at al. using a new geometrical method [15] and by Kohout at al. extracting blood-vessel skeleton [16]. In [17], a novel mathematical formalization of a well-known class of geometric primitives, namely generalized cylinders was developed for image segmentation. The detection of PE in CTA images is a challenging research area for several research groups. In previous works, firstly lung and lung vessel segmentation were achieved to detect PE.

The most important problem is the distinction of PE from the tissue as it has the same intensity values. Only a few attempts have been made to find the discriminating features. Masutani et al. recently presented a method for emboli detection based on lung vessel segmentation and to distinguish PE, proposed to use the intensity, local contrast, length, and volume of a PE [18]. Pichon et al. used the size and the intensity in a special way. The intensities inside a vessel were projected on the vessel surface by computing the first quartile of intensities on a ray between the surface and the medial axis of a vessel [19]. Zhou et al. used the features based on intensity, edge strength, length, volume, and the shape of a candidate in relation to the local vessel [20,21]. Bouma et al. recognized that intensity and shape are not the properties of distinction for PE and proposed to use the shape of a vessel and the shape of lumen inside vessels, as new features for the classification of PE in the CTA images [22]. Besides in [23–26], model-based cardiac diagnoses of pulmonary embolism were developed and their methods were clinically validated on animal data sets for PE.

In the earlier works, the properties such as intensity, size and presumed shape of PE have been used to distinguish PE with different tissues. However, there is not any constant shape of PEs. It can be regionally anywhere in the vessel tree. It is not considered as a PE if smaller than a certain size; it can have various sizes. So in this paper, a new CAD system for automatic detection of PE in CTA images has been proposed. In order to use at vessel segmentation, some reference points (RP) have been detected by making use of the properties of unchangeable anatomical structure. PEs are differentiated from the other tissues having the same intensity, such as the heart or different lung disease tissues except for PE thanks to RPs. We have used 33 positive data sets which have 450 PEs. These numbers are high for data sets and PEs. The results at the end of these processes have been analysed by the performance measures which are used in medical image evaluation and compared to the previous works. It has been observed that the performance of the method for PE detection in this paper is better than the ones in literature and the proposed CAD system is found quite useful to use as a second reader by the radiologists [27].

2. Materials and methods

In this work, experimental data was collected from Dr. Siyami Ersek thoracic and cardiovascular surgery training and research hospital. All pulmonary computed tomographic angiography exams were performed with 16 detectors CT (Somatom Sensation 16, Siemens, AG, Erlangen, Germany) equipment. Patients were informed about the examination and also for breath holding. Imaging was performed with Bolus tracking program. After scenogram, single slice was taken at the level of pulmonary trunk. A bolus tracking was placed at pulmonary trunk and trigger was adjusted to 100 HU (Hounsfield Unit). 70 ml non-ionic contrast agent at the rate of 4 mL/s with an automated syringe (Optistat Contrast Delivery System, Liebel-Flarsheim, USA) was used. When opacification was reached at the pre-adjusted level, the exam was performed from the supraclavicular region to the diaphragms. Contrast injection was performed via 18–20G intra venous cannula that was placed at antecubital vein. Scanning parameters were 120 kV, 80–120 mA, slice thickness 1 mm, pitch 1.0–1.2. Images were reconstructed with 1 mm and 5 mm thickness, and evaluated at mediastinal window (WW 300, WL 50) with advanced workstation (Wizard, Siemens, AG, Erlangen, Germany) in coronal, sagittal and axial planes. Oblique plans were used when needed. Each exam consisted of 400–500 images with 512×512 voxels and 0.8 mm resolution. Data sets belonging to 33 patients with 15 female and 18 male were used. Ages of females varied between 31 and 80 and ages of males varied between 40 and 79.

To detect pulmonary embolism, firstly, lung vessel segmentation was performed. Here, lung vessel segmentation was a key point, because the performance of detecting PE directly depended on the correctness of vessel segmentation. The vessel segmentation, developed in this work, was categorized into three steps. The first step was pulmonary trunk and left – right pulmonary artery (TLRPA) segmentation, the second step was lobar and segmental vessel segmentation, and the last step was subsegmental vessel segmentation. Lung segmentation was a necessary process used in the beginning phase of the vessel segmentation. Therefore, lungs and mediastinum were separated and used in vessel segmentation steps. The first step was performed in mediastinum, the second step in the lung and mediastinum, and the third step in the lung. The detailed flow chart of this method is shown in Fig. 1.

2.1. *Lung segmentation and mediastinum detection*

In lung segmentation, initially, each image has been thresholded using −300 HU as the level of threshold. The voxels smaller than the threshold level were removed from the image. To remove vessels from the lung region and to attain the lung as a whole, the vessels in lung region were removed by discarding the small objects with the help of Connected Component Labeling (CCL) algorithm. At the last step, lung regions were segmented according to the volumes of the components of the image.

In the CTAI, to detect mediastinum region (MR) in each slice, minimum and maximum points of lung region were obtained and, X_{min}, X_{max}, Y_{min}, and Y_{max} values were designated. These values indicated the corner of the rectangle border. Mediastinum region was determined as a rectangle which was reduced 10 voxels inward from each side of the rectangle border of the lung region (Fig. 2).

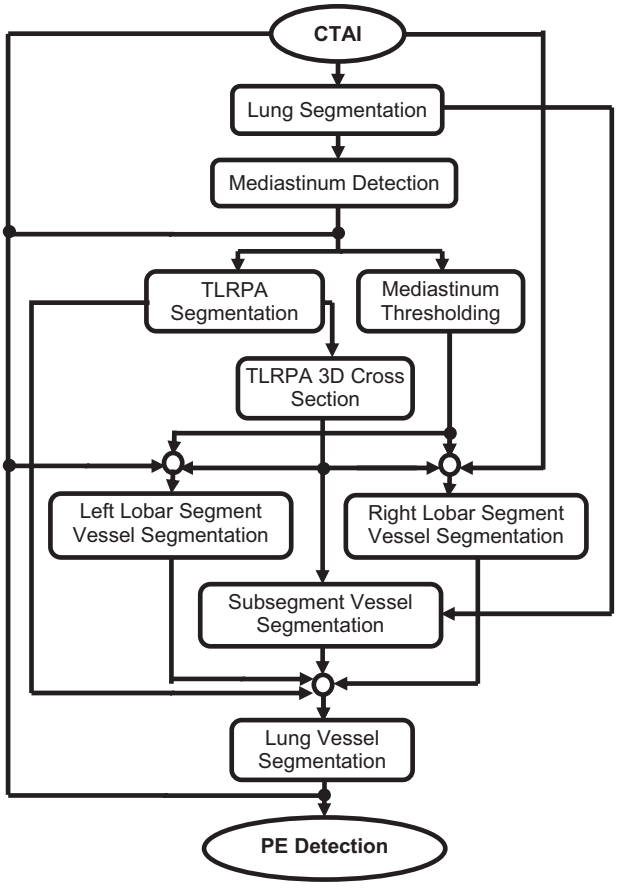

Fig. 1 – Flow chart of the proposed method for pulmonary embolism detection including lung segmentation and lung vessel segmentation.

Fig. 2 – Detection of mediastinum region. The borders of segmented lungs are shown by external rectangle. The mediastinum region between left and right lungs is shown by internal rectangle.

2.2. *Pulmonary trunk, left pulmonary artery, right pulmonary artery segmentation*

In this section, to segment of TLRPA, initially, each image was thresholded using 300 HU < Image < 500 HU as the level of threshold. In the case of inaccurate scans, as a solution, 300 HU threshold value could be lowered but in this case, pulmonary artery could not be segmented by itself. Therefore, threshold level below 300 HU was not suitable. In this study, accurate CTA scans were considered. Then components outside the MR were removed and the small gaps on the components were filled with region growing method. The images were labeled by CCL as 2D, and components with less than 300 number of voxels, were removed from the image. In a similar manner, the images were labeled by CCL as 3D and all the components except the biggest one were removed from the image. Ascending aorta (AscA), descending aorta (DesA), superior vena cava (SVC) were segmented and removed from the images (AscA, DesA and SVC segmentations were explained in Section 2.4.1). In Fig. 3a the original image, in Fig. 3b 2D, TLRPA detected by applied method were shown.

If there is not any PE in lung vessels, the vessels properly continue from the pulmonary trunk forward to the left-right pulmonary artery. However, if there is a PE in the lung, vessel structure does not regularly continue due to the low-threshold value of the PE. The detection of the first spoiling points of the vessel structure was covered in Section 2.2.1.

2.2.1. *Pulmonary trunk, left pulmonary artery, right pulmonary artery 3D cross section detection*

The values of X, Y and Z coordinates of each voxel belonging to TLRPA in Section 2.2 were loaded to three vectors. Then, starting from Y_{min}, 3D cross sections of TLRPA were taken with 5 voxel intervals to Y_{max}. The number of voxels of each cross section was counted and each of them was subtracted from the consecutive one. Starting from the pulmonary trunk, the differences between the cross sections in left and right pulmonary arteries had similar values if there was not any PE. However, if the difference between the consecutive cross sections was large, the corrupted cross section due to PE was encountered. The Y values of first corrupted cross sections in the left and right pulmonary arteries were detected as the starting points of PE. We called these points as 1st reference point (RP) if it was on the right pulmonary artery and 2nd RP if it was on the left pulmonary artery as seen in Fig. 4a and b.

2.3. *Mediastinum thresholding*

In this section, we thresholded mediastinum region so as to be used at segmentation. First, components which were outside of the MR were removed from the images. Then each image was thresholded using 150 HU < Image < 500 HU for the vessel, and 1 HU < Image < 150 HU for PE as the level of threshold and two difference images were obtained. Components were labeled by CCL as 2D and if the number of voxels was under 1000, then they were removed from the images obtained for the vessel. Images of TLRPA acquired from Section 2.2 with two images obtained for the vessel and for PE from this section were gathered. The resulting image is given in Fig. 5.

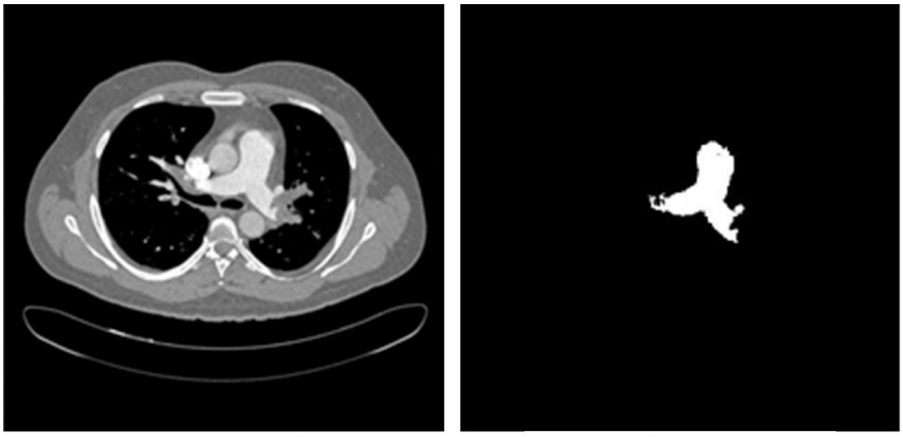

Fig. 3 – Segmentation of pulmonary trunk, left pulmonary artery and right pulmonary artery. (a) The original image belongs to a patient. (b) Segmented pulmonary trunk + left pulmonary artery + right pulmonary artery.

The PE region following TLRPA can be seen more detailed in Fig. 4. TLRPA carried out at the end of gathering is seen in white because of its value of 2 and other parts are seen in grey because of their value of 1.

2.4. *Lobar and segmental vessel segmentation*

This section was completed at three steps. First, some reference points were detected to use in segmentation. Second, right and left mediastinum region lobar, segmental vessel segmentation were achieved and lastly right and left lobar segmental vessel segmentation between the pulmonary vein and the end of MR were achieved.

2.4.1. *Ascending aorta, descending aorta, superior vena cava segmentation and reference points detection*

In this section, some reference points were determined in order to use in segmentation. In 2D images, the places of 1-AscA, 2-DesA, 3-SVC and 4-TLRPA were shown in Fig. 6. SVC shown with number 3 in Fig. 6 was used to detect the right reference points (RRP) since right lobar segmental vessel (RLSV) could be segmented at every patient. In order to be able to detect the RRP, firstly, locations of SVC's were detected from the image beginning of pulmonary trunk to the end of left pulmonary artery in each 2D image. For this, each image was thresholded using Image > 500 HU as the level of threshold because HU of SVC was very high. Then X_{min} of SVC in each of 2D image was called as 3rd RP and Y_{min} as 4th RP. The middle point in X dimension value of component SVC was defined as 5th RP for each of 2D images (Fig. 7). Y_{max} point of cross section of 5th RP in X dimension in right lung image was detected as 6th RP (Fig. 8). DesA shown with number 2 in Fig. 6 was used to detect the left reference points (LRP) since left lobar segmental vessel (LLSV) could be segmented at the every patient. DesA were detected from the image beginning of pulmonary trunk to the pulmonary vein in each 2D image in our previous work [28]. Then X_{min} of DesA was called as 7th RP and Y_{max} as 8th RP in each of 2D images (Fig. 9).

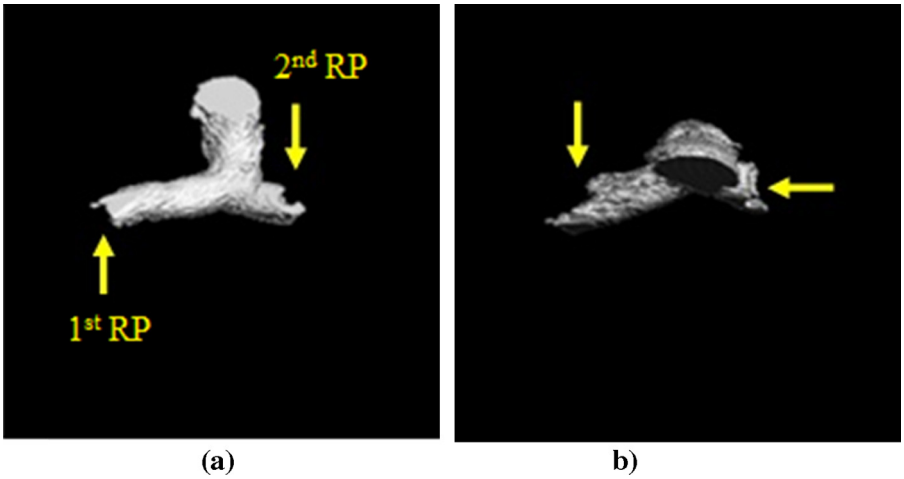

Fig. 4 – Determining of 1st, 2nd RPs. (a) 3D Images of TLRPA rendered from 2D images in Fig. 3b (front view) (b) top view of (a). Since left and right pulmonary arteries have PEs, the vessels structure does not continue smoothly. The arrows show first corrupted points in both pulmonary arteries. The left first point is called as 1st RP and the right first point is called as 2nd RP.

Fig. 5 – Thresholded mediastinum regions. This image is acquired gathering three different images to use in segmentation of vessel with PEs. One of them is a thresholded image with vessel threshold level in MR, another one is a thresholded image with PE threshold level in MR and the last one is 2D TLRPA shown in Fig. 3b.

Image of heart appears while 2D CTAI were proceeding to the ends and the heart gets bigger towards the number 1 lung region as seen in Fig. 10b. During expanding, it was seen that the lobar segmental vessels were under the expanding point shown with an arrow in Fig. 10a. So 9th RP and 10th RP were found from mentioned expanding point. In images, to detect the expanding point, firstly, the region between the 3rd RP and 7th RP of number 1 lung in Fig. 10b was taken and loaded to a new image (Fig. 10c). Secondly, Y_{min} of the image in Fig. 10c and X_{max} of the cross section in Y_{min} were detected. Here X_{max} was called as 9th RP and Y_{min} as 10th RP. This method was applied to all of the images from the beginning image of pulmonary trunk to the end image of the lobar segmental vessels and detected reference points were loaded to a vector with the image numbers.

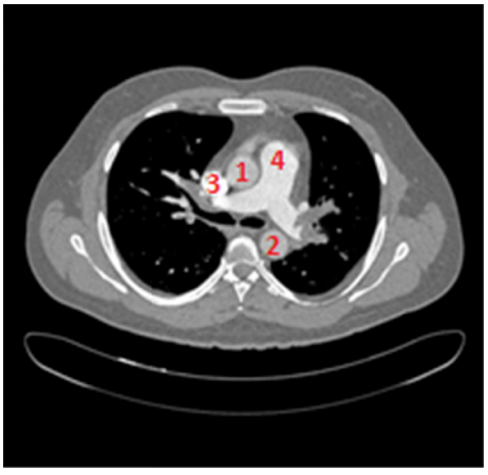

Fig. 6 – The shown numbers are (1) ascending aorta, (2) descending aorta, (3) superior vena cava and (4) pulmonary trunk and left–right pulmonary artery on the original image.

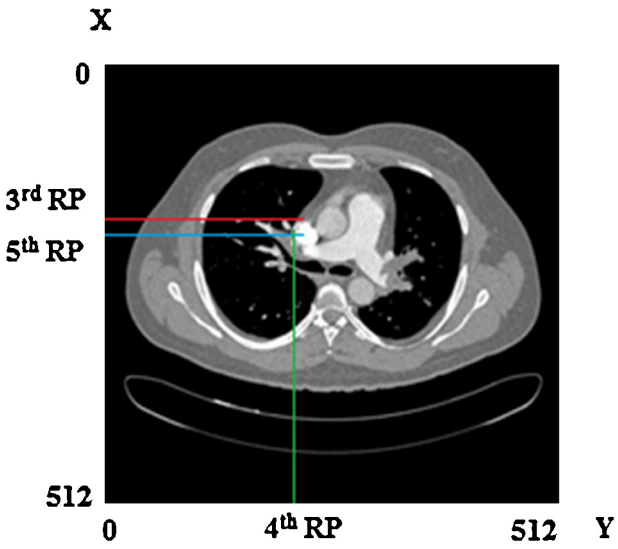

Fig. 7 – Determining of 3rd, 4th and 5th RPs. In the image X and Y coordinates and sizes are shown. X_{min} of predetermined SVC is 3rd RP, $(X_{max} - X_{min})/2$ of SVC is 5th RP and Y_{min} of SVC is 4th RP.

2.4.2. Mediastinum region lobar, segmental vessel segmentation

In this section, RLSV and LLSV were separately determined. Firstly, to segment PE, blocking the vessel, segmentation was carried out. For this, all of the components that were in right side of 1st RP detected in Section 2.2.1 for RLSV, and all of the components that were in left side of 2nd RP for LLSV were removed from the thresholded MR image detected in Section 2.3. Secondly, the vessels following at the end points of PE were segmented. For this, the left side of 4th RP for RLSV, and the right side of 2nd RP for LLSV for each images were thresholded using 150 HU < Image < 500 HU as the level of threshold. Then the regions outside MR were removed from the images.

Fig. 8 – Determining of 6th RPs. Y_{max} point of cross section of 5th RP in X coordinate in right lung image is 6th RP.

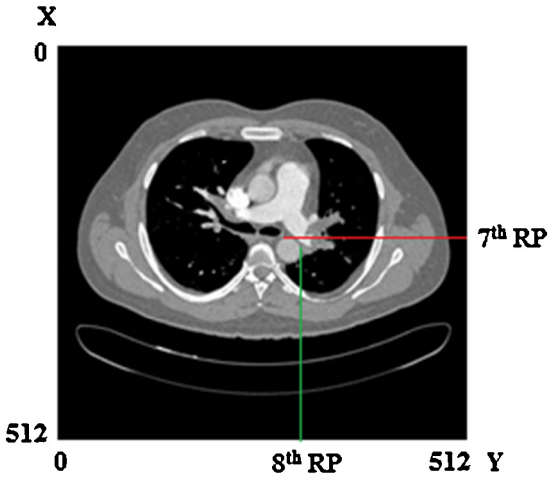

Fig. 9 – Determining of 7th and 8th RPs. In the image X and Y coordinates and sizes are shown. X_{min} of predetermined DesA is 7th RP and Y_{max} of DesA is 8th RP.

Fig. 11 – Complete lung vessel 2D image which is carried out combining pulmonary trunk, left–right pulmonary arteries, lobar, segment and subsegment vessels.

Lastly, mediastinum region RLSV, and LLSV segmentation was achieved by gathering the images which were detected at the first and second steps.

2.4.3. *Lobar segmental vessel segmentation between the pulmonary vein and the end of MR*

TLRPA and lobar segmental vessels in MR continue from lung region and they connect to the heart with the pulmonary vein towards the end of 2D images. RLSV and LLSV were separately determined in this section too. To segment, RLSV and LLSV proceed towards into the lung out of MR, firstly, each images primarily was thresholded using 1 HU < Image < 500 HU as the level of threshold. Then, the components except MR were removed from these images. Then, the region in the right side of 6th RP with the smaller part than 3rd RP in X dimension for RLSV and the region in the left side of 8th RP with the smaller part than 9th RP in X dimension for LLSV were removed from the image thresholded in Section 2.3. So, RLSV and LLSV segmentation from the outside of the MR to the pulmonary vein was achieved.

2.5. *Subsegmental vessel segmentation*

The small components in the lung region were determined as subsegmental vessel. For this the components were labeled by CCL as 2D, and if their voxel numbers were under 100, they were detected to be subsegmental vessel.

2.6. *Lung vessel segmentation*

The results in Sections 2.2, 2.4 and 2.5 were gathered to achieve the exact lung vessel segmentation. The last formed image was the total vessel image. One of the 2D total vessel images can be seen in Fig. 11 and 3D images rendered from the 2D images can be seen in Fig. 12.

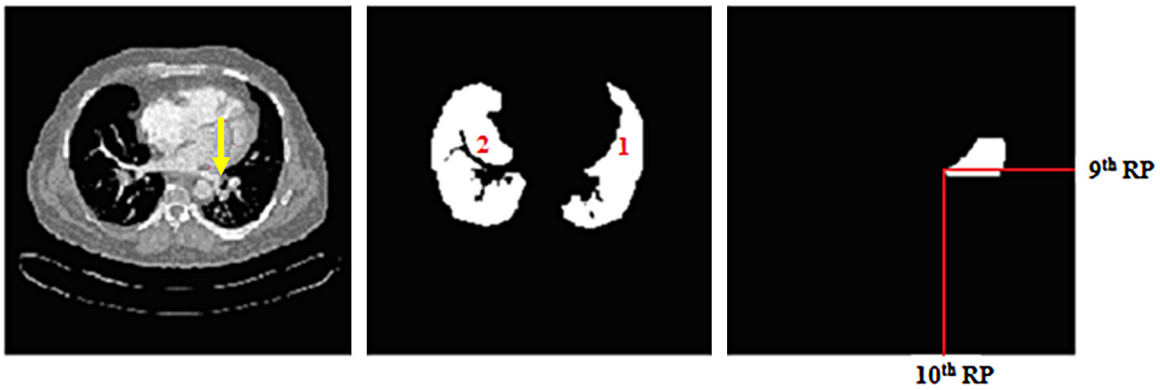

Fig. 10 – Determining of 9th and 10th RPs. (a) The original 2D image which includes heart. The heart gets bigger towards the left lung region. During the heart expanding towards the end of 2D slice, lobar segment vessels stay under the expanding point. This expanding point is shown with an arrow. (b) Segmented left and right lung images. Left lung image shown with number 1 gets smaller from top to the expanding point (c) The region between the 3rd RP and 7th RP of left lung is taken than 9th and 10th RPs are defined from the expanding point. X_{max} of the cross section in Y_{min} of the expanding point is called as 9th RP. Y_{min} of the expanding point is called as 10th RP.

Fig. 12 – 3D lung vessel tree image rendered from 2D images shown in Fig. 11.

2.7. *Pulmonary embolism detection*

First of all, three chest radiologists having various experiences analyzed the CTA data sets of 33 patients together. One of the radiologists had 3 years of experience, the second one had 7 years of experience and the last one had 10 years of experience. They decided that three and two agreements were PE and at least two disagreements were not PE. The number of PEs having three agreements was 422, two agreements was 23, two disagreements which were not considered as PEs was 17. CAD system detected the 5 of 17 two disagreements as PEs. The radiologists read the data sets with the help of CAD system again and they confirmed the mentioned 5 candidates as PEs too. So, the radiologists detected the 445 PEs before CAD system and they fixed the number of PEs as 450 by using CAD system.

Then, to detect PEs correctly with CAD system, firstly, components in 3D vessel tree were labeled using 3D CCL algorithm and unconnected components were removed. Secondly, every 3D lung vessel tree was thresholded using 1 HU < Image < 150 HU as the level of threshold. These components were the candidates of PE. Some of these candidates were not PE and they caused an increase in the number of False Positive (FP), such as lung diseases except PE, the partial-volume effect on the vessel, lymphoid tissue, noise, and motion artifacts. Low number of FP and high number of true positive (TP) were the key points of the system performance.

In this study, to reduce the FP rate three methods were applied to the candidates. (1) Very small particles were assumed as noise (because of partial-volume effect) and removed using 3×3 median filtering. (2) If any candidate was located only in one slice, it was removed. (3) PE occludes the vessel completely or partially, thus, its shape was like a lump rather than a thin line. Therefore, thin-line shaped candidates were removed by computing the shape factor. To determine the shape factor of any candidate, first, the dimensions of the smallest lump, which can include the candidate, was obtained. Then, the ratio of the lump volume to the candidate volume, called the shape factor, was obtained. If this ratio was close to zero, this means that the candidate had a thin line shape.

Finally, different volume thresholds were applied to the PE candidates to determine the FROC curve. The levels of volume threshold were 6.4 mm^3, 9.6 mm^3, 16 mm^3, 48 mm^3, 64 mm^3, and 80 mm^3. The components having small volumes were removed. So the remaining components were designated as PE. Detected PEs were labeled by 3D CCL and compared with the PEs determined by the radiologists. Then numbers of TP, FP and False Negative (FN) were counted manually. In Table 1, the numbers of TP, FP and FN belonging to 33 patients were given.

3. Results

PEs belonging to a patient and marked with arrows manually by the radiologists, are shown in Fig. 13a. The 2D lung

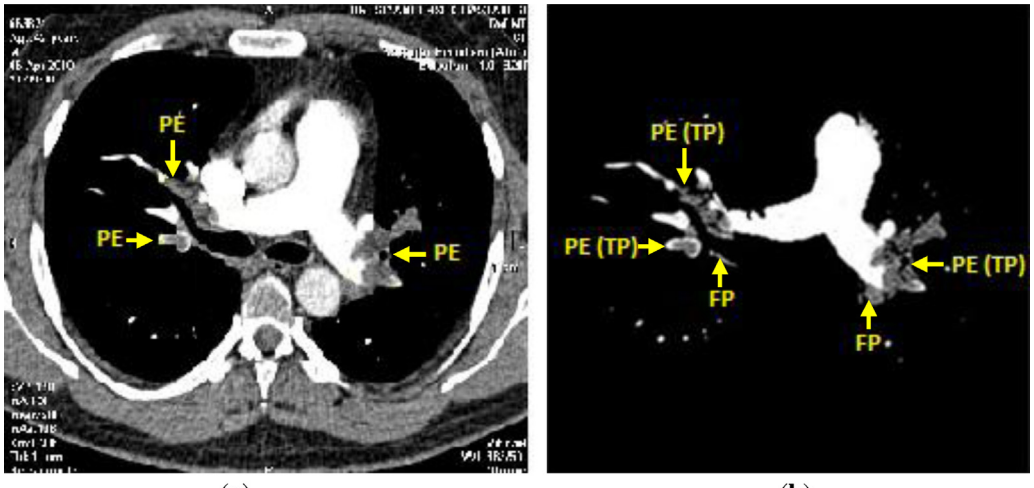

(a) (b)

Fig. 13 – Results of manual and CAD detection. (a) Manual detection of pulmonary embolism by the radiologists. Three PEs can be seen at the lobar and segment vessels (b) 2D lung vessel tree and PEs obtained from the CAD system. According to the developed CAD system, three PEs are determined as TP, also two components are determined as FP since they are not PE.

Table 1 – Results of CAD system according to the level of volume thresholds for 33 patients having 450 PEs. Some of PE candidates are PE and they are called as TP, some of them are not PE and they are called as FP. The PEs which are not detected are called as FN.

	Level of volume threshold					
	6.4 mm^3	9.6 mm^3	16 mm^3	48 mm^3	64 mm^3	80 mm^3
TP	428	419	403	385	321	275
FN	22	31	47	65	129	175
FP	476	430	409	385	322	271

Table 2 – The results of our CAD system and the results of the previous studies. The number of PE, the number of data sets (ds), Sensitivity, FP/ds and remark are shown.

Reference	PE	ds	Sensitivity (%)	FP/ds	Remark
Masutani [18]	21	11	100	7.7	Low PE
Pichon [19]	22	3	86	6.3	Low PE
Das [29]	168seg	33	88	4	Only peripheral PE
	120sub		78		
Digumarthy [30]	270	39	92	2.8	No motion No diseases
Maizlin [31]	45	8	58	6.4	Low Sens. %, Low ds
Kiraly [32]	69	8	50	–	Low Sens. %
Zhou [20]	225	14	52	11.4	Low Sens. %
Buhmann [33]	352	40	47	3.9	Low Sens. %
Wittenberg [34]	38	119	95	3.8	Low PE
Bouma [22]	116	19	58	4.0	Disease; 22% additional
			63	4.9	PE
			73	15	
Proposed method	450	33	61	8.2	Patients who have lung
			95	14.4	diseases except PE

vessel tree image with the PEs, which were detected as a result of the proposed method, is seen with their real HU values in Fig. 13b. The components, indicated as TP, are PEs identified by the radiologists. The components which are indicated as FP are not PEs. Detected 3 TPs and 2 FPs can be seen in Fig. 13b.

In the proposed method, 428 of 450 PEs determined by the radiologists from 33 patients, were detected. Detection sensitivity was adjusted by changing the volume threshold of the PE candidates to evaluate the performance of the method and the average number of FP/ds was counted. Using 6.4 mm^3 volume threshold, the sensitivity was 95% at 14.4 FP/ds, and 90% of sensitivity was obtained at 12.4 FP/ds using 16 mm^3 volume threshold and 61% of sensitivity at 8.2 FP/ds was obtained for 80 mm^3 volume threshold. PEs in subsegmental vessels cannot be detected by using high volume thresholds. Therefore, detection sensitivity and FP/ds decrease and only large PEs are detected. If small volume thresholds are used, small PEs can be detected in addition to large PEs. Thus, sensitivity and FP/ds rate increase. The results at the end of these processes have been analyzed by the performance measures which are used in medical image evaluation. Fig. 14 shows the FROC curve for this detection test.

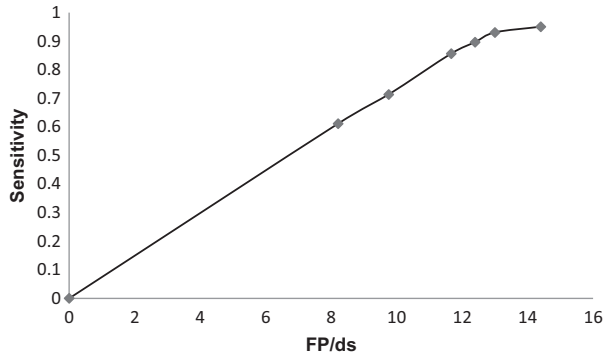

Fig. 14 – FROC graph of 33 patients. Each point is acquired due to the volume threshold. Using a 6.4 mm^3 volume threshold, the sensitivity was 0.95 with 14.4 FP/ds, and we obtained 0.90 sensitivity with 12.4 FP/ds using a 16 mm^3 volume threshold the number of false positives was 8.2 per data sets at a 80 mm^3 volume threshold with 0.61 sensitivity. When the level of volume threshold gets lower, the sensitivity and FP/ds value increase. When the level of volume threshold gets bigger, the sensitivity and FP/ds value decrease.

4. Discussion and conclusion

The comparison of the results of the method proposed in this study and the results of the previous studies are provided in Table 2. As can be seen in Table 2, Masutani et al. have achieved a result of high sensitivity in their work but they have detected low number of PEs from a few data sets. Similarly, Pichon et al. have detected low number of PEs from only three patients. Sensitivity in their study is lower than that of the proposed method in this work. Das et al. have used the same number of data sets as in this study. Their number of PEs is high, but it is not possible to compare their PE detection performance with ours, because they detect the PEs only in the segmental and subsegmental vessels. Digumarthy et al. have had high sensitivity with high data sets, but they have used the data sets which have no other disease except for PEs. Although,

the data sets from patients with heart or lung diseases except for PE have been used in this work, sensitivity of proposed method is higher than that of their study. However, FP/ds is a bit higher than their works, too. Maizlin et al. have had lower number of PEs, and lower number of data sets than our work, but their sensitivity is lower than that of our study. Zhou et al. and Kiraly et al. have had lower number of data sets and lower number of PEs than our study, however their sensitivities are low. Also Buhmann et al. have had higher number of data sets and lower number of PEs than our study, however their sensitivity is low. The FP/ds in our study is worse than these three works, but if these FP/ds values are evaluated according to the number of data sets and number of PEs, this is an acceptable result. When compared according to FP/ds, it should be expected that FP rate is high when the number of PEs is low. For example, patient number 31 in our data sets has only 3 PEs. The result of the CAD system for this patient is TP = 3 and FP = 15, 14, 14, 13 for 16 mm^3, 48 mm^3, 64 mm^3, 80 mm^3 volume threshold values respectively. As mentioned by Araoz et al. in a panel discussion, the rate of positive pulmonary CTAs is in the range of 5–10% in most studies [1]. Therefore, a high FP rate is relevant in the case of having less number of PEs or absence of PE. Wittenberg et al. have had higher data sets but lower number of PEs than our work. Their sensitivity value is the same as ours but if the sensitivity is evaluated according to the number of PEs, it can be seen that the result of our work is more confidential. Also their FP/ds value is better than that of our study since the number of PEs in their work is lower than that of our work. Bouma et al. have detected 20% more PEs than the radiologists had detected before, then they have made the radiologists approve the last result but the minimum and maximum sensitivity and minimum and maximum FP/ds are worse than those of our work. As a result, it has been observed that the performance of the method for PE detection in this paper is better than the ones in literature and the proposed CAD system is found quite useful to use as a second reader by the radiologists.

Conflict of interest

The authors declare that there is no conflict of interest.

Acknowledgements

This work has been supported by Dr. Siyami Ersek Thoracic and Cardiovascular Surgery Training and Research Hospital, Istanbul, Turkey. The authors wish to thank chief of staff in the hospital, Prof. Dr. Ibrahim Yekeler.

REFERENCES

[1] P.A. Araoz, L.B. Haramati, J.R. Mayo, E.J. Barbosa Jr., F.J. Rybicki, et al., Panel discussion: pulmonary embolism imaging and outcomes, AJR American Journal of Roentgenology 198 (6) (2012) 1313–1319, http://dx.doi.org/10.2214/AJR.11.8461.

[2] M. Domingo, L. Martí-Bonmatí, R. Dosdá, Y. Pallardó, Interobserver agreement in the diagnosis of pulmonary embolism with helical CT, European Journal of Radiology 34 (2000) 136–140.

[3] E. Coche, S. Pawlak, S. Dechambre, B. Maldague, Peripheral pulmonary arteries: identification at multi-slice spiral CT with 3D reconstruction, European Radiology 13 (2003) 815–822.

[4] B. Ghaye, D. Szapiro, I. Mastora, V. Delannoy, A. Duhamel, J. Remy, et al., Peripheral pulmonary arteries: how far in the lung does multi-detector row spiral CT allow analysis? Radiology 219 (2001) 629–636.

[5] J.M. Remy, J. Remy, D. Artaud, F. Deschildre, A. Duhamel, Peripheral pulmonary arteries: optimization of the spiral CT acquisition protocol, Radiology 204 (1997) 157–163.

[6] U.J. Schoepf, P. Costello, CT angiography for diagnosis of pulmonary embolism: state of the art, Radiology 230 (2004) 329–337.

[7] P.D. Stein, S.E. Fowler, L.R. Goodman, A. Gottschalk, C.A. Hales, D. Russell, et al., Multidetector computed tomography for acute pulmonary embolism, New England Journal of Medicine 354 (2006) 2317–2327.

[8] U. Schoepf, M.A. Kessler, C.T. Rieger, P. Herzog, E. Klotz, S. Wiesgigl, et al., Multislice CT imaging of pulmonary embolism, European Radiology 11 (11) (2001) 2278–2286.

[9] F. Calle-Alonso, C.J. Pérez, J.P. Arias-Nicolás, J. Martín, Computer-aided diagnosis system: a Bayesian hybrid classification method, Computer Methods and Programs in Biomedicine 112 (2013) 104–113.

[10] W.J. Choi, T.S. Choi, Automated pulmonary nodule detection based on three-dimensional shape-based feature descriptor, Computer Methods and Programs in Biomedicine 113 (2014) 37–54.

[11] J.R.F.S. Sousa, A.C. Silva, A.C. Paiva, R.A. Nudes, Methodology for automatic detection of lung nodules in computerized tomography images, Computer Methods and Programs in Biomedicine 98 (2010) 1–14.

[12] J. Kuruvilla, K. Gunavathi, Lung cancer classification using neural networks for CT images, Computer Methods and Programs in Biomedicine 113 (2014) 202–209.

[13] M. Hassan, A. Chaudhry, A. Khan, J.Y. Kim, Carotid artery image segmentation using modified spatial fuzzy c-means and ensemble clustering, Computer Methods and Programs in Biomedicine 108 (2012) 1261–1276.

[14] R. Rocha, A. Campilho, J. Silva, E. Azevedo, R. Santos, Segmentation of ultrasound images of the carotid using RANSAC and cubic splines, Computer Methods and Programs in Biomedicine 101 (2011) 94–106.

[15] C. Zohios, G. Kossioris, Y. Papaharilaou, Geometrical methods for level set based abdominal aortic aneurysm thrombus and outer wall 2D image segmentation, Computer Methods and Programs in Biomedicine 107 (2012) 202–217.

[16] J. Kohout, A. Chiarini, G.J. Clapworthy, G. Klajnsek, Aneurysm identification by analysis of the blood-vessel skeleton, Computer Methods and Programs in Biomedicine 109 (2013) 32–47.

[17] K.K. Delibasis, A. Kechriniotis, I. Maglogiannis, A novel tool for segmenting 3D medical images based on generalized cylinders and active surfaces, Computer Methods and Programs in Biomedicine 111 (2013) 148–165.

[18] Y. Masutani, H. MacMahon, K. Doi, Computerized detection of pulmonary embolism in spiral CT angiography based on volumetric image analysis, IEEE Transactions on Medical Imaging 21 (2002) 1517–1523.

[19] E. Pichon, C.L. Novak, A.P. Kiraly, D.P. Naidich, A novel method for pulmonary emboli visualization from high-resolution CT images, Proceedings of the SPIE Medical Imaging 5367 (2004) 161–170.

[20] C. Zhou, H.P. Chan, S. Patel, P.N. Cascade, B. Sahiner, L.M. Hadjiiski, et al., Preliminary investigation of computer-aided

detection of pulmonary embolism in 3-D CT pulmonary angiography, Academic Radiology 12 (6) (2005) 782–792.
[21] C. Zhou, L.M. Hadjiiski, B. Sahiner, H.P. Chan, S. Patel, P.N. Cascade, et al., Computerized detection of pulmonary embolism in 3-D CT images: vessel tracking and segmentation techniques, Proceedings of the SPIE Medical Imaging 5032 (2003) 1613–1620.
[22] H. Bouma, J.J. Sonnemans, A. Vilanova, F.A. Gerritsen, Automatic detection of pulmonary embolism in CTA images, IEEE Transactions on Medical Imaging 28 (8) (2009) 1223–1230.
[23] C. Starfinger, C.E. Hann, J.G. Chase, T. Desaive, A. Ghuysen, G.M. Shaw, Model-based cardiac diagnosis of pulmonary embolism, Computer Methods and Programs in Biomedicine 87 (2007) 46–60.
[24] J.A. Revie, D.J. Stevenson, J.G. Chase, C.E. Hann, B.C. Lambermont, A. Ghuysen, et al., Validation of subject-specific cardiovascular system models from porcine measurements, Computer Methods and Programs in Biomedicine 109 (2013) 197–210.
[25] C.E. Hann, J. Revie, D. Stevenson, S. Heldmann, T. Desaive, C.B. Froissart, et al., Patient specific identification of the cardiac driver function in a cardiovascular system model, Computer Methods and Programs in Biomedicine 101 (2011) 201–207.
[26] C.E. Hann, J.G. Chase, T. Desaive, C.B. Froissart, J. Revie, D. Stevenson, et al., Unique parameter identification for cardiac diagnosis in critical care using minimal data sets, Computer Methods and Programs in Biomedicine 99 (2010) 75–87.
[27] H. Özkan, Computer Aided Detection of Pulmonary Embolism in Computed Tomography Angiography Images (PhD thesis), Sakarya University, Turkey, 2011 (in Turkish).
[28] H. Özkan, Segmentation of ascending and descending aorta in CTA images, World Academy of Science Engineering and Technology (ICBCBBE 2012) 65 (2012) 451–453.
[29] M. Das, A. Schneider, U. Schoepf, J. Cheema, S. Wood, P. Costello, et al., Computer-aided diagnosis of peripheral pulmonary emboli, Chicago, November 30-December 5, Radiological Society of North America (RSNA) program book (2003) 351–352, C02–C232.
[30] S.R. Digumarthy, C.R. Kagay, A.C. Legasto, V.V. Muse, C. Wittram, J.O. Shepard, Computer-aided detection (CAD) of acute pulmonary emboli: evaluation in patients without significant pulmonary disease, Chicago, IL, 2006, SSC04-08.
[31] Z. Maizlin, P. Vos, M. Gody, P. Cooperberg, Computer-aided detection of pulmonary embolism on CT angiography: initial experience, Journal of Thoracic Imaging 22 (4) (2007) 324–329.
[32] A.P. Kiraly, C.L. Novak, D.P. Naidich, I. Vlahos, J.P. Ko, G.T. Brusca-Augello, A comparison of 2D and 3D evaluation methods for pulmonary embolism detection in CT images, Proceedings of the SPIE 6146, Medical Imaging 2006: Image Perception, Observer Performance, and Technology Assessment 61460H (March) (2006), http://dx.doi.org/10.1117/12.652430.
[33] S. Buhmann, P. Herzog, J. Stoeckel, M. Salganicoff, M. Wolf, M.F. Reiser, et al., Clinical evaluation of a CAD prototype for the detection of pulmonary embolism, in: European Congress of Radiology, 2006, p. B-585.
[34] R. Wittenberg, J.F. Peters, I.A.H. van den Berk, N.J.M. Frelin, R. Lely, B. Hoop, et al., Computed tomography pulmonary angiography in acute pulmonary embolism, the effect of a computer-assisted detection prototype used as a concurrent reader, Journal of Thoracic Imaging 28 (2013) 315–321.